The Astrophysical Journal, 935:116 (10pp), 2022 August 20 https://doi.org/10.3847/1538-4357/ac8056

Limits on X-Ray Polarization at the Core of Centaurus A as Observed with the Imaging X-Ray Polarimetry Explorer

Steven R. Ehlert[1], Riccardo Ferrazzoli[2], Andrea Marinucci[3], Herman L. Marshall[4], Riccardo Middei[5,6], Luigi Pacciani[7], Matteo Perri[5,6], Pierre-Olivier Petrucci[8], Simonetta Puccetti[3], Thibault Barnouin[9], Stefano Bianchi[10], Ioannis Liodakis[11], Grzegorz Madejski[12], Frédéric Marin[9], Alan P. Marscher[13], Giorgio Matt[10], Juri Poutanen[14,15], Kinwah Wu[16], Iván Agudo[17], Lucio A. Antonelli[5,18], Matteo Bachetti[19], Luca Baldini[20,21], Wayne H. Baumgartner[1], Ronaldo Bellazzini[20], Stephen D. Bongiorno[1], Raffaella Bonino[22,23], Alessandro Brez[20], Niccoló Bucciantini[24,25,26], Fiamma Capitanio[2], Simone Castellano[20], Elisabetta Cavazzuti[27], Stefano Ciprini[5,28], Enrico Costa[2], Alessandra De Rosa[2], Ettore Del Monte[2], Laura Di Gesu[27], Niccoló Di Lalla[29], Alessandro Di Marco[2], Immacolata Donnarumma[27], Victor Doroshenko[15,30], Michal Dovčiak[31], Teruaki Enoto[32], Yuri Evangelista[2], Sergio Fabiani[2], Javier A. Garcia[33], Shuichi Gunji[34], Kiyoshi Hayashida[35], Jeremy Heyl[36], Wataru Iwakiri[37], Svetlana G. Jorstad[13,38], Vladimir Karas[31], Takao Kitaguchi[32], Jeffery J. Kolodziejczak[1], Henric Krawczynski[39], Fabio La Monaca[2], Luca Latronico[22], Simone Maldera[22], Alberto Manfreda[20], Francesco Massaro[22,23], Ikuyuki Mitsuishi[40], Tsunefumi Mizuno[41], Fabio Muleri[2], Michela Negro[42,43,44], C.-Y. Ng[45], Stephen L. O'Dell[1], Nicola Omodei[29], Chiara Oppedisano[22], Alessandro Papitto[18], George G. Pavlov[46], Abel L. Peirson[29], Melissa Pesce-Rollins[20], Maura Pilia[19], Andrea Possenti[19], Brian D. Ramsey[1], John Rankin[2], Ajay Ratheesh[2], Roger W. Romani[29], Carmelo Sgrò[20], Patrick Slane[47], Paolo Soffitta[2], Gloria Spandre[20], Toru Tamagawa[32], Fabrizio Tavecchio[48], Roberto Taverna[49], Yuzuru Tawara[40], Allyn F. Tennant[1], Nicholas E. Thomas[1], Francesco Tombesi[28,50,51], Alessio Trois[19], Sergey Tsygankov[14,15], Roberto Turolla[16,49], Jacco Vink[52], Martin C. Weisskopf[1], Fei Xie[53], Silvia Zane[16]
(IXPE Collaboration),
James Rodi[2], Elisabeth Jourdain[54], and Jean-Pierre Roques[54]
[1] NASA Marshall Space Flight Center, Huntsville, AL 35812, USA; steven.r.ehlert@nasa.gov
[2] INAF Istituto di Astrofisica e Planetologia Spaziali, Via del Fosso del Cavaliere 100, I-00133 Roma, Italy
[3] Agenzia Spaziale Italiana, Via del Politecnico snc, I-00133 Roma, Italy
[4] MIT Kavli Institute for Astrophysics and Space Research, Massachusetts Institute of Technology, 77 Massachusetts Avenue, Cambridge, MA 02139, USA
[5] Space Science Data Center, Agenzia Spaziale Italiana, Via del Politecnico snc, I-00133 Roma, Italy
[6] INAF Osservatorio Astronomico di Roma, Via Frascati 33, I-00040 Monte Porzio Catone (RM), Italy
[7] Istituto di Astrofisica e Planetologia Spaziali—Istituto Nazionale di Astrofisica (IAPS-INAF), Via Fosso del Cavaliere, 100—I-00133, Rome, Italy
[8] Université Grenoble Alpes, CNRS, IPAG, F-38000 Grenoble, France
[9] Université de Strasbourg, CNRS, Observatoire Astronomique de Strasbourg, UMR 7550, F-67000 Strasbourg, France
[10] Dipartimento di Matematica e Fisica, Università degli Studi Roma Tre, Via della Vasca Navale 84, I-00146 Roma, Italy
[11] Finnish Centre for Astronomy with ESO, University of Turku, Vesilinnantie 5, FI-20014 Turku, Finland
[12] SLAC National Accelerator Laboratory 2575 Sand Hill Road, Menlo Park, CA 94025, USA
[13] Institute for Astrophysical Research, Boston University, 725 Commonwealth Avenue, Boston, MA 02215, USA
[14] Department of Physics and Astronomy, FI-20014 University of Turku, Finland
[15] Space Research Institute of the Russian Academy of Sciences, Profsoyuznaya Str. 84/32, Moscow 117997, Russia
[16] Mullard Space Science Laboratory, University College London, Holmbury St Mary, Dorking, Surrey RH5 6NT, UK
[17] Instituto de Astrofísicade Andalucía, IAA-CSIC, Glorieta de la Astronomía s/n, E-18008 Granada, Spain
[18] INAF Osservatorio Astronomico di Roma, Via Frascati 33, I-00078 Monte Porzio Catone (RM), Italy
[19] INAF Osservatorio Astronomico di Cagliari, Via della Scienza 5, I-09047 Selargius (CA), Italy
[20] Istituto Nazionale di Fisica Nucleare, Sezione di Pisa, Largo B. Pontecorvo 3, I-56127 Pisa, Italy
[21] Dipartimento di Fisica, Università di Pisa, Largo B. Pontecorvo 3, I-56127 Pisa, Italy
[22] Istituto Nazionale di Fisica Nucleare, Sezione di Torino, Via Pietro Giuria 1, I-10125 Torino, Italy
[23] Dipartimento di Fisica, Università degli Studi di Torino, Via Pietro Giuria 1, I-10125 Torino, Italy
[24] INAF Osservatorio Astrofisico di Arcetri, Largo Enrico Fermi 5, I-50125 Firenze, Italy
[25] Dipartimento di Fisica e Astronomia, Università degli Studi di Firenze, Via Sansone 1, I-50019 Sesto Fiorentino (FI), Italy
[26] Istituto Nazionale di Fisica Nucleare, Sezione di Firenze, Via Sansone 1, I-50019 Sesto Fiorentino (FI), Italy
[27] ASI—Agenzia Spaziale Italiana, Via del Politecnico snc, I-00133 Roma, Italy
[28] Istituto Nazionale di Fisica Nucleare, Sezione di Roma "Tor Vergata," Via della Ricerca Scientifica 1, I-00133 Roma, Italy
[29] Department of Physics and Kavli Institute for Particle Astrophysics and Cosmology, Stanford University, Stanford, California 94305, USA
[30] Institut für Astronomie und Astrophysik, Universität Tübingen, Sand 1, D-72076 Tübingen, Germany
[31] Astronomical Institute of the Czech Academy of Sciences, Boční II 1401/1, 14100 Praha 4, Czech Republic
[32] RIKEN Cluster for Pioneering Research, 2-1 Hirosawa, Wako, Saitama 351-0198, Japan
[33] California Institute of Technology, Pasadena, CA 91125, USA
[34] Yamagata University, 1-4-12 Kojirakawa-machi, Yamagata-shi 990-8560, Japan
[35] Osaka University, 1-1 Yamadaoka, Suita, Osaka 565-0871, Japan
[36] University of British Columbia, Vancouver, BC V6T 1Z4, Canada
[37] Department of Physics, Faculty of Science and Engineering, Chuo University, 1-13-27 Kasuga, Bunkyo-ku, Tokyo 112-8551, Japan
[38] Department of Astrophysics, St. Petersburg State University, Universitetsky pr. 28, Petrodvoretz, 198504 St. Petersburg, Russia
[39] Physics Department and McDonnell Center for the Space Sciences, Washington University in St. Louis, St. Louis, MO 63130, USA
[40] Graduate School of Science, Division of Particle and Astrophysical Science, Nagoya University, Furo-cho, Chikusa-ku, Nagoya, Aichi 464-8602, Japan
[41] Hiroshima Astrophysical Science Center, Hiroshima University, 1-3-1 Kagamiyama, Higashi-Hiroshima, Hiroshima 739-8526, Japan
[42] University of Maryland, Baltimore County, Baltimore, MD 21250, USA
[43] NASA Goddard Space Flight Center, Greenbelt, MD 20771, USA
[44] Center for Research and Exploration in Space Science and Technology, NASA/GSFC, Greenbelt, MD 20771, USA

[45] Department of Physics, The University of Hong Kong, Pokfulam, Hong Kong
[46] Department of Astronomy and Astrophysics, Pennsylvania State University, University Park, PA 16802, USA
[47] Center for Astrophysics, Harvard & Smithsonian, 60 Garden Street, Cambridge, MA 02138, USA
[48] INAF Osservatorio Astronomico di Brera, Via E. Bianchi 46, I-23807 Merate (LC), Italy
[49] Dipartimento di Fisica e Astronomia, Università degli Studi di Padova, Via Marzolo 8, I-35131 Padova, Italy
[50] Dipartimento di Fisica, Università egli Studi di Roma "Tor Vergata," Via della Ricerca Scientifica 1, I-00133 Roma, Italy
[51] Department of Astronomy, University of Maryland, College Park, Maryland 20742, USA
[52] Anton Pannekoek Institute for Astronomy & GRAPPA, University of Amsterdam, Science Park 904, 1098 XH Amsterdam, The Netherlands
[53] Guangxi Key Laboratory for Relativistic Astrophysics, School of Physical Science and Technology, Guangxi University, Nanning 530004, People's Republic of China
[54] CNRS, Institut de Recherche en Astrophysique et Planétologie (IRAP), 9 Av. colonel Roche, BP 44346, F-31028 Toulouse cedex 4, France
Received 2022 June 2; revised 2022 July 8; accepted 2022 July 10; published 2022 August 22

Abstract

We present measurements of the polarization of X-rays in the 2–8 keV band from the nucleus of the radio galaxy Centaurus A (Cen A), using a 100 ks observation from the Imaging X-ray Polarimetry Explorer (IXPE). Nearly simultaneous observations of Cen A were also taken with the Swift, NuSTAR, and INTEGRAL observatories. No statistically significant degree of polarization is detected with IXPE. These observations have a minimum detectable polarization at 99% confidence (MDP_{99}) of 6.5% using a weighted, spectral model-independent calculation in the 2–8 keV band. The polarization angle ψ is consequently unconstrained. Spectral fitting across three orders of magnitude in X-ray energy (0.3–400 keV) demonstrates that the SED of Cen A is well described by a simple power law with moderate intrinsic absorption ($N_{\mathrm{H}} \sim 10^{23}\,\mathrm{cm}^{-2}$) and a Fe K$\alpha$ emission line, although a second unabsorbed power law is required to account for the observed spectrum at energies below 2 keV. This spectrum suggests that the reprocessing material responsible for this emission line is optically thin and distant from the central black hole. Our upper limits on the X-ray polarization are consistent with the predictions of Compton scattering, although the specific seed photon population responsible for the production of the X-rays cannot be identified. The low polarization degree, variability in the core emission, and the relative lack of variability in the Fe Kα emission line support a picture where electrons are accelerated in a region of highly disordered magnetic fields surrounding the innermost jet.

Unified Astronomy Thesaurus concepts: Polarimetry (1278); X-ray quasars (1821); Radio galaxies (1343)

1. Introduction

Particle acceleration is ubiquitous in astrophysical systems, with charged particles routinely being accelerated to energies orders of magnitude larger than those attainable in terrestrial experiments. Supermassive black holes ($M \gtrsim 10^6 M_\odot$) at the centers of galaxies are known to be among the most prominent particle acceleration sites in the universe, although details of the acceleration and radiative mechanisms in active galactic nuclei (AGN) remain ambiguous: multiple models of these processes can fit the spectral energy distributions (SEDs) of AGN equally well. Polarimetry, which more directly constrains the magnetic field geometry of the regions where acceleration takes place, is able to break many of these degeneracies. Polarization measurements of high-energy, nonthermal emission provide an additional means to determine the radiative processes and the nature of the populations of energetic particles that produce them.

Centaurus A is the most nearby radio galaxy ($z = 0.0018$, $D = 3.84$ Mpc), and the radio jets in its nucleus have been studied in great detail. Radio observations of the core of Cen A indicate complex velocity and polarization structures. Long-term observations of Cen A with Very Long Baseline Interferometry (VLBI, Tingay et al. 2001; Müller et al. 2014) suggest that within the central $\sim$1 pc the jets have an apparent velocity (normalized to the speed of light) of $\beta \sim 0.12$, with a jet viewing angle of $\sim$12°–45° with respect to the line of sight. On larger scales of $\sim$100 pc, Hardcastle et al. (2003) measured apparent velocities of $\beta \sim 0.5$. Cen A has also recently been resolved on an angular scale of 25 μarcsec at a wavelength of 1.3 mm with the Event Horizon Telescope (EHT, Janssen et al. 2021). These observations reveal both an edge-brightened jet northeast of the core and a fainter counter-jet to the southwest. The surface brightness structure of these jets is interpreted in Janssen et al. (2021) as evidence of a helical magnetic field wrapped around the jets. The jet and counter-jet each have two branches that are clearly separated from one another. For the jet these two branches have position angles of 43° and 52° (measured eastward from the north), which is nearly identical to the jet position angle on larger scales (55° ± 7°; e.g., Schreier et al. 1979; Burns et al. 1983; Jones et al. 1996). X-ray observations of the nucleus of Cen A with Chandra and XMM-Newton show that the X-rays are mainly generated within a small region around the nucleus, as the core has previously been measured to vary in luminosity by $\sim$60% on timescales of $\sim$20 days (Evans et al. 2004). A distance of 20 light days ($\sim$0.0168 pc) corresponds to an angular scale of $\sim$0.″001 at the distance of Cen A, far smaller than the best angular resolution provided by Chandra ($\sim$0.″5) for X-ray imaging but well matched to the resolution of the EHT radio observations. The position angle of the inner radio jet can therefore be compared with the electric vector position angle (EVPA, itself perpendicular to the local magnetic field) of Cen A.

Measurements of radio polarization by Burns et al. (1983) at 6 cm show that the polarization degree varies between $\sim$5% and 20% in different regions in the vicinity of the nucleus, although the nucleus itself is only polarized at the 0.21% ± 0.01% level. The core region of Cen A was measured to have a polarization of 0.46% ± 0.03% at 20 cm in the same study. The morphology of the polarization vectors throughout

the larger scale (∼100 pc) jet regions suggests that the magnetic field lines are consistently parallel to the jet axis, with no evidence of field lines transverse to the jet near its outer edges (Clarke et al. 1986; Hardcastle et al. 2003). More recent ALMA results find that the core of Cen A has no measurable polarization at 221 GHz (Goddi et al. 2021), with a 3σ upper limit to the linear polarization of 0.09%. Far-infrared polarimetry with SOFIA/HAWC+ (89 μm) measured polarization of $1.5\% \pm 0.2\%$ with an EVPA of $151^\circ \pm 4^\circ$, consistent with dichroic absorption and emission (Lopez-Rodriguez 2021). After correction for the stellar component of the host galaxy, the $\sim 1''$ core of Cen A was previously observed to have a polarization degree of $\sim 11.1\% \pm 0.2\%$ at a wavelength of ~ 2 μm (Capetti et al. 2000), with an EVPA of 148° east of north, which is perpendicular to the jet position angle.

Past observations have shown that the X-ray spectrum is affected by absorption below ∼10 keV, with a column density of $N_{\rm H} \sim 10^{23}$ cm^{-2}. At hard X-rays the continuum photon flux is characterized by a power law with slope $\Gamma \sim 1.8$ (e.g., Fürst et al. 2016, and references therein). The presence of a narrow Fe K emission line, combined with the absence of a strong Compton hump, suggests reflection from Compton-thin material. The detection of a high-energy cutoff or continuum curvature from hard X-ray satellites such as CGRO/OSSE, Suzaku, INTEGRAL, and NuSTAR (Kinzer et al. 1995; Steinle et al. 1998; Markowitz et al. 2007; Beckmann et al. 2011; Fürst et al. 2016), is under debate, which prevents an unambiguous determination of the origin of the primary X-ray emission. It could be dominated either by thermal Compton emission from a hot X-ray "corona," as in radio-quiet AGN (Stern et al. 1995; Zdziarski et al. 1997, 2000), or by nonthermal emission from the base of the jet, or a combination of the two.

Here we report polarimetric observations of Cen A obtained with the Imaging X-ray Polarimetry Explorer (IXPE), a NASA mission in partnership with the Italian Space Agency (ASI). As described in detail elsewhere (Weisskopf et al. 2022 and references therein), IXPE includes three identical X-ray telescopes, each comprising an X-ray mirror assembly and a polarization-sensitive pixelated detector (Soffitta et al. 2021), to provide imaging polarimetry over a nominal 2–8 keV band. IXPE data telemetered to ground stations in Malindi (primary) and in Singapore (secondary) are transmitted to the Mission Operations Center (MOC, at the Laboratory for Atmospheric and Space Physics, University of Colorado) and then to the Science Operations Center (SOC, at NASA Marshall Space Flight Center). The SOC processes science and relevant engineering and ancillary data to produce data products that are archived at the High-Energy Astrophysics Science Archive Research Center (HEASARC, at NASA Goddard Space Flight Center) for use by the international astrophysics community. Cen A was observed for a net exposure time of 100 ks from 2022 February 15 (01:00 UT) to 17 (13:00 UT).

In addition to the IXPE observations, Cen A was also observed simultaneously (or nearly simultaneously) by the NuSTAR, Swift, and INTEGRAL missions in order to provide broadband (∼0.3–400 keV) measurements of the X-ray spectrum.

2. Observations

IXPE observations of Cen A were taken starting at 00:00 UTC on 2022 February 15. Simultaneous (or nearly so) observations with other X-ray telescopes are summarized in Table 1. Operational constraints limited the ability of NuSTAR and Swift to observe Cen A simultaneously with IXPE. Given that Cen A has not been previously observed to exhibit substantial variability in the X-rays on timescales of days, we do not anticipate this offset in time to introduce any major systematic errors in our joint spectral analysis. The light curve during each of these observations also shows no evidence for significant intraobservation variability in the emission from Cen A.

2.1. IXPE

We refer interested readers to Weisskopf et al. (2016, 2022) for a complete description of the hardware deployed upon IXPE and its performance, and here only summarize the most relevant details for this work. IXPE data were processed using a pipeline that applies estimates of the photoelectron emission direction (and hence the polarization), location, and energy of each event after applying corrections for charging effects, detector temperature, and gas electron multiplier (GEM) to gain nonuniformity. Spurious modulation is removed using the algorithm of Rankin et al. (2022).

The output of this pipeline processing is an event file for each of the three IXPE Detector Units (DUs) that contains, in addition to the typical information related to spatially resolved X-ray astronomy, the event-by-event Stokes parameters, from which the polarization of the radiation can be derived. In addition to the standard pipeline processing for IXPE data, three additional corrections were applied to the data: small time-dependent changes to the gain correction obtained from data taken with the onboard calibration sources (Ferrazzoli et al. 2020) close to the actual time of observation; further corrections to the aspect solution to remove apparent positional shifts in sources arising from small motions of the IXPE boom; and the weights of each event, updated to reflect the results of Di Marco et al. (2022) and to fix a known error in the data processing pipeline at the time of processing.

Analysis of the processed IXPE event lists utilizing both weighted and unweighted data was carried out with multiple independent analysis tools, most notably `ixpeobssim` (Baldini et al. 2022). The `ixpeobssim` software suite was designed specifically to operate with both simulated and real IXPE data; Baldini et al. (2022) describe these algorithms in detail. For Cen A, the core region was filtered from the rest of the event list by using a $1'$ radius aperture[55] around the centroid of the X-ray data.

We have attempted to measure the polarization degree and angle and their uncertainties along with the minimum detectable polarization at 99% confidence ($\rm MDP_{99}$) of the region using several different techniques in order to test the robustness of the final result. The simplest calculation was performed with a polarization cube, which is constructed using the *xpbin* tool on the selected event list with the PCUBE algorithm. The polarization properties and their uncertainties were calculated according to the equations contained in Kislat et al. (2015). No treatment of the expected background counts in the source region was performed for this calculation. Estimates derived from multiple source-free regions of the sky using an identical $1'$ radius aperture suggest that background is <10% of the total counts within the source aperture. We have constructed two polarization cubes from these observations—one that utilizes the event-specific weights and one that does not.

[55] This radius corresponds to ∼2 half-power diameters for the IXPE optics.

Table 1
Observational Log of the X-Ray Telescope Observations

Mission	Obs ID	Energy keV	Start Date (YYYY-MM-DD)	End Date (YYYY-MM-DD)	Exposure (ks)
IXPE	01004301	2–8	2022-02-15	2022-02-17	100
NuSTAR	60701033002	5–70	2022-02-17	2022-02-17	20.8
NuSTAR	10802601002	5–70	2022-02-18	2022-02-18	23.1
Swift	00096451017	0.3–8	2022-02-24	2022-02-25	0.59
Swift	00096451018	0.3–8	2022-02-25	2022-02-25	1.4
INTEGRAL/ISGRI		30–400	2022-02-11	2022-02-18	144
INTEGRAL/SPI		20–400	2022-01-11	2022-02-18	672

Spectropolarimetric fitting was also used to determine the polarization degree and angle of the Cen A core. Spectra were extracted using the *xpbin* tool on the same event list by using the PHA algorithm to create OGIP-compliant spectra for the total (Stokes I) and Stokes Q/U parameters. For the spectral extraction, a local source-free circular aperture with a radius of $1'$ was used to construct background Stokes spectra. Two variants of the nine IXPE spectra (3 detectors $\times$ $I/Q/U$ spectra per detector) were produced: one variant that includes the event weights and a second that does not. In this paper all references to spectropolarimetric fitting will be based on the unweighted spectra. Tests using the weighted spectra have confirmed that both sets of spectra result in upper limits to the polarization, with no meaningful differences between them. We have also confirmed that the best-fit spectral model parameters (including polarization) are not sensitive to the particular choice of the background region.

As a further independent check of the polarization measurements, we also utilized a maximum-likelihood calculation of the polarization degree and angle based on the method developed by Marshall (2021) to allow for background selected from a separate region (Marshall, in prep). Background events are accounted for in a manner similar to the calculations in Elsner et al. (2012), although this new calculation explicitly assumes Poisson rather than Gaussian statistics as assumed in Elsner et al. (2012). These calculations were developed and executed independently of `ixpeobssim`. The unweighted energy-dependent modulation factor $\mu(E)$ from Di Marco et al. (2022) was used, and no events were excluded from the calculation. For this calculation, the background was estimated from an annular region 160″–320″ from the core.

2.2. NuSTAR

To calibrate and clean the NuSTAR data, we used the NuSTAR Data Analysis Software (`NuSTARDAS`, v. 2.1.1). We derived level 2 cleaned event files with the `nupipeline` task, while high-level scientific data products were extracted using the `nuproducts` tool. The latest calibration data files in the NuSTAR CALDB (version 20220301) were used. These data have a significantly lower count rate than the data analyzed in Fürst et al. (2016). Our measured count rate for Cen A in the 3–70 keV energy band is $\sim 4\,\mathrm{ct\,s^{-1}}$, which is a factor of $\sim$4 lower than the value quoted for the 2013 NuSTAR observation (Fürst et al. 2016). A 70″ radius circular region (corresponding to a 90% enclosed energy fraction of the NuSTAR point-spread function) was used to extract the source spectrum.[56] A concentric annulus with inner and outer radii of 210″ and 270″ was then adopted to estimate the background, which subtends a solid angle a factor of 2 larger than the 120″ radius circle used for the background region in Fürst et al. (2016). FPMA/B spectra were then binned to achieve a signal-to-noise ratio (S/N) larger than 10 in each spectral channel.

2.3. Swift

Swift-XRT observations were performed in Windowed Timing (WT) mode, and the data were processed using the X-Ray Telescope Data Analysis Software (`XRTDAS`, v. 3.6.1). As for NuSTAR data, we used the latest calibration files available in the Swift/XRT CALDB (version 20210915). The X-ray source spectrum was extracted from the cleaned event file using a circular region with a radius of 20 pixels ($\sim$46″). This region corresponds to a 90% enclosed energy fraction of the Swift point-spread function. The background was extracted using a circular region of 20 pixel radius from a blank sky WT observation available in the Swift archive. Finally, the 0.3–10 keV source spectra were binned, requiring each spectral channel to have at least 25 counts.

2.4. INTEGRAL

The INTEGRAL observations used in these analyses are part of a multiepoch program. The data reported here consists of exposures that followed a 5×5 dithering pattern. Data contaminated by solar flares and pointings affected by Earth's radiation belt have been removed.

The SPI data from 2022 January 11 to February 18 have been processed through the SPIDAI interface.[57] Cen A was assumed to be the only source in the sky model, and constant during the exposure duration. Due to the evolution of the background over the entire data set, its normalization was determined on a $\sim$1 hr timescale. The spectrum was constructed in 21 channels from 20 to 500 keV and averaged over the exposure. Tests comparing the full SPI data set to the SPI spectrum extracted for a time window immediately before and after IXPE observations show no significant differences in count rate for any channel. We therefore choose to utilize data taken throughout this entire time window to maximize the spectrum's S/N, especially for the highest energy channels.

The ISGRI data between 2022 February 11–18 were processed using the Off-line Science Analysis 11.2 version (OSA11.2), resulting in a total useful duration of 144.4 ks. The source was considered constant on an $\sim$1800 s timescale. The

[56] We note that this source aperture is slightly smaller than the 100″ radius used for spectral extraction in Fürst et al. (2016), but this discrepancy alone cannot account for the lower count rate we measure.

[57] Interface developed at IRAP to analyze SPI data, publicly available at http://sigma-2.cesr.fr/integral/spidai; see description in Burke et al. (2014).

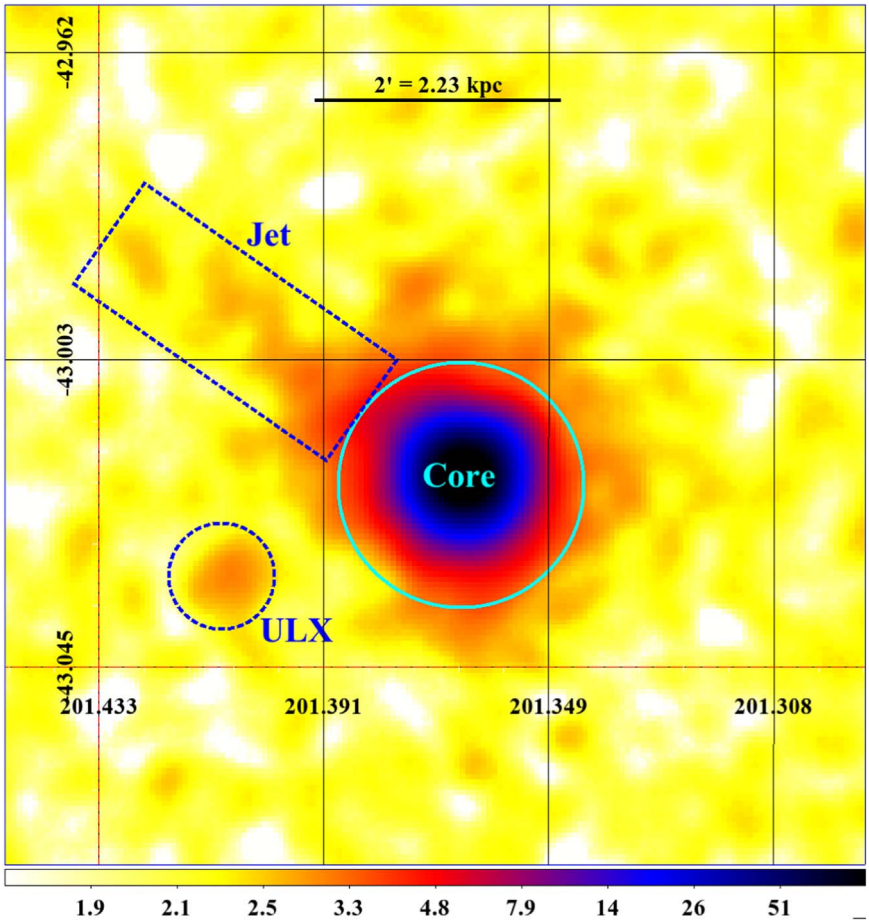

Figure 1. Image of Cen A constructed using the data from all three IXPE detectors. The image has been smoothed using a Gaussian with a width of $\sigma = 3$ pixels and a radius of 6 pixels. The regions used to calculate the MDP_{99} of the jet and ULX regions are shown in a blue dashed box and circle, respectively. The cyan region is the $1'$ aperture surrounding the core used for investigating the polarization of the core.

spectrum was averaged over the observing period and binned into 29 channels in the 30–1000 keV energy range.

3. Results

Figure 1 displays the combined image of Cen A resulting from data obtained with all three IXPE detectors. Three regions of interest are shown in this figure: the core, the X-ray jet, and a previously identified ultraluminous X-ray source (ULX) to the southeast of the core. Between all three detectors, a total of 28,179 (source + background) counts were detected in the core region, 2147 in the jet, and 469 in the vicinity of the ULX. This work will focus on the core region but briefly discuss upper limits to X-ray polarization in the other two regions as well.

3.1. Polarization

Figure 2 presents the Stokes Q and U maps of the IXPE field of view, along with polar plots showing the limits on the broadband polarization of Cen A's core. In addition to the core region, two other sources are considered. Neither the X-ray jets nor the ultraluminous X-ray source (ULX) near the core of Cen A have sufficient counts to measure statistically significant X-ray polarization. The broadband polarization of the jet region has an MDP_{99} of 40%, while $MDP_{99} = 80\%$ for the ULX region. Using the weighted polarization cubes gives MDP_{99} values of 36% and 73% for the jet and ULX regions, respectively. These values of MDP_{99} all correspond to the optimistic assumption that all events within these regions originate from the sources and not the background. Given the low S/N of the imaging data, the polarization of these two sources is effectively unconstrained. Using the likelihood base method that accounts for background (see Section 2.1) from a region at a comparable distance from the core but on the west side of it, the polarization of jet and ULX cannot be established even if they were fully polarized (MDPs are 100%). Fitting the broadband (2–8 keV) polarization data of the Cen A core (without weighting), then combining the data from all three telescopes simultaneously, gives no statistically significant polarization signal above $MDP_{99} = 7.2\%$. Incorporating the weights into the calculation provides a stricter limit of $MDP_{99} = 6.5\%$. Dividing the IXPE data into smaller energy bins also does not yield any statistically significant polarization in any of the energy bands investigated.

3.2. Spectral Fitting

We have modeled the broadband (0.5–400 keV) Swift + IXPE[58] + NuSTAR + INTEGRAL X-ray spectrum of the core of Cen A with several simple yet physically motivated models. The broadband emission above 2 keV (the lower-energy bound of the IXPE data) can be well described by a simple power-law continuum plus a Gaussian-shaped Fe Kα emission line with

[58] For this spectral fit, no polarization information from IXPE was utilized, only the Stokes I parameter spectrum.

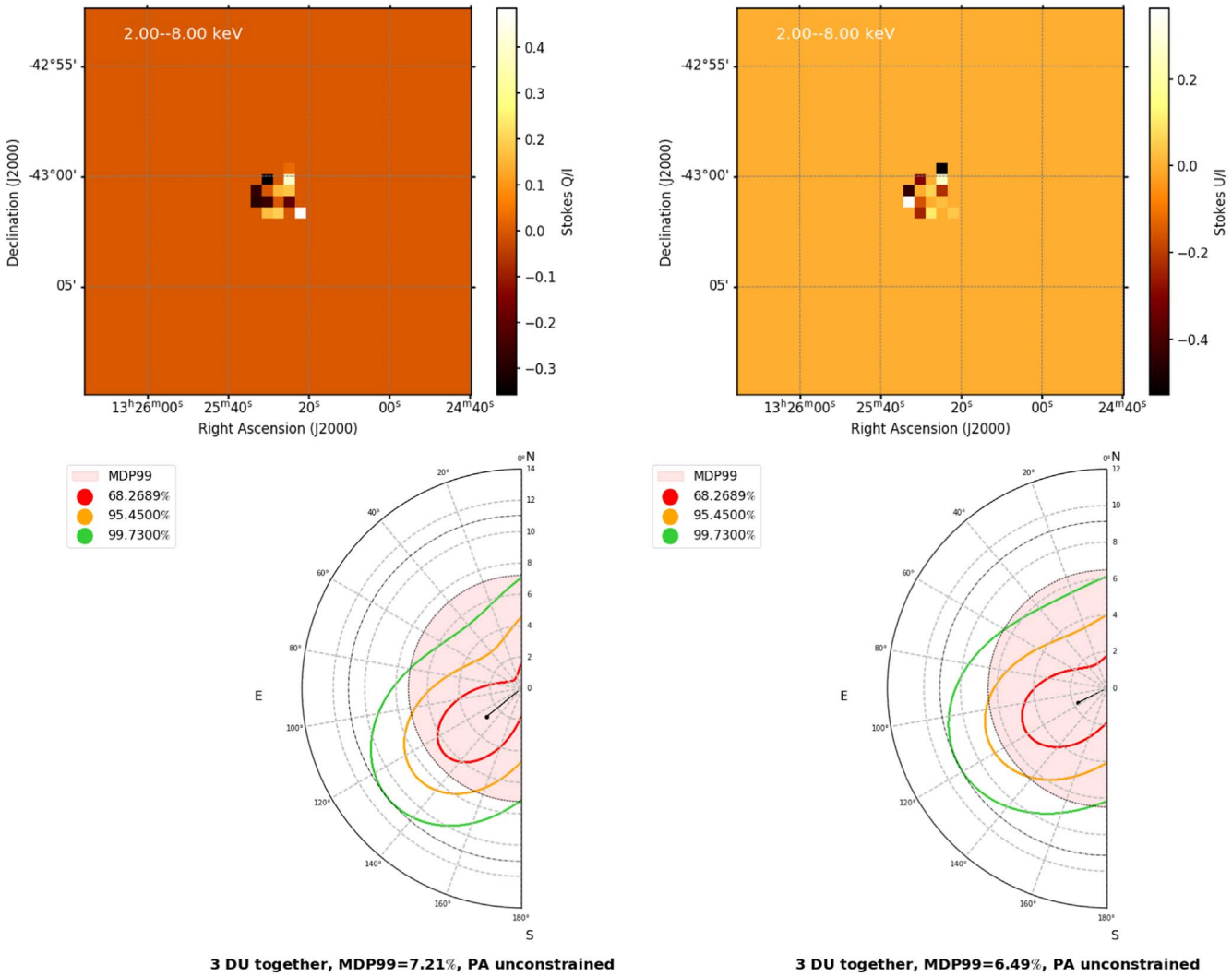

Figure 2. Maps of the X-ray polarization in the core of Cen A. All of these subfigures utilize the combined results of all three IXPE detectors in the 2–8 keV energy band. Top left: normalized Stokes Q within the core region. Top right: normalized Stokes U within the core region. Bottom left: polar plot of the X-ray polarization in the core region derived without event weighting. Red, orange, and green contours denote the 68.3%, 95.5%, and 99.7% confidence intervals for the polarization degree and angle. The red shaded region is the MDP at 99% confidence. Bottom right: polar plot of the X-ray polarization derived using event weights. No statistically significant X-ray polarization is observed using either weighting method.

moderate intrinsic absorption ($\sim 10^{23}$ cm^{-2}). There is no apparent evidence of a high-energy cutoff within the INTEGRAL data out to 400 keV. The spectrum below 2 keV shows strong evidence for another spectral component beyond a single intrinsically absorbed power law. The presence of the Fe Kα line and the absence of a statistically significant Compton hump suggest that the observed spectrum originates in reflection from an optically thin plasma. Unless otherwise noted, all uncertainties correspond to 90% ($\Delta\chi^2 = 2.706$) confidence intervals, and all upper limits correspond to 99% ($\Delta\chi^2 = 6.635$) confidence.

Our primary model fit was performed using `XSPEC` version 12.12.1 (Arnaud 1996) and assumes an intrinsically absorbed cutoff power law, a second power law with only Galactic absorption, and a Gaussian emission line (`const*tbabs* (ztbabs* (zcutoffpl + zgauss) + pow)` in `XSPEC`). We assume zero intrinsic width for the Fe Kα line and a Galactic absorption column density of $N_{\rm H} = 2.36 \times 10^{20}$ cm^{-2} (HI4PI Collaboration et al. 2016). Our best-fit photon index for this model is $\Gamma = 1.88 \pm 0.03$. The best-fit intrinsic absorption column density is $1.48^{+0.05}_{-0.04} \times 10^{23}$ cm^{-2}, and the cutoff energy is $E_{\rm cut} > 500$ keV (the hard limit of this parameter in the `zcutoffpl` model in `XSPEC`). The cross-calibration constants for the various detectors differ from IXPE Detector Unit 1 by $< 10\%$ for the other two IXPE detectors, $\sim$30% for the NuSTAR FPMA/FPMB spectra, $\sim$10%–15% for the Swift-XRT spectra, and $\sim$40%–60% for the INTEGRAL SPI/ISGRI spectra. The overall fit statistic of this model ($\chi^2 = 1188$ for 1134 degrees of freedom) suggests that this model is a good fit to the data. The resultant model fit and its residuals can be found in Figure 3.

The line energy and flux of the Fe Kα line are only slightly lower than the NuSTAR-derived values quoted in Fürst et al. (2016). The line energy we measure is $E_{\rm Fe} = 6.33 \pm 0.04$ keV (cf. 6.40 keV in Fürst et al. 2016) and the total flux of the line is $(2.27 \pm 0.23) \times 10^{-4}$ ph cm^{-2} s^{-1} (see $(2.88 \pm 0.22) \times 10^{-4}$ ph cm^{-2} s^{-1} in Fürst et al. 2016). We conclude that the flux of the Fe Kα line has remained constant despite the factor of $\sim$3 drop in the overall flux of the Cen A core. The measured Fe Kα flux is also consistent with results from past observations

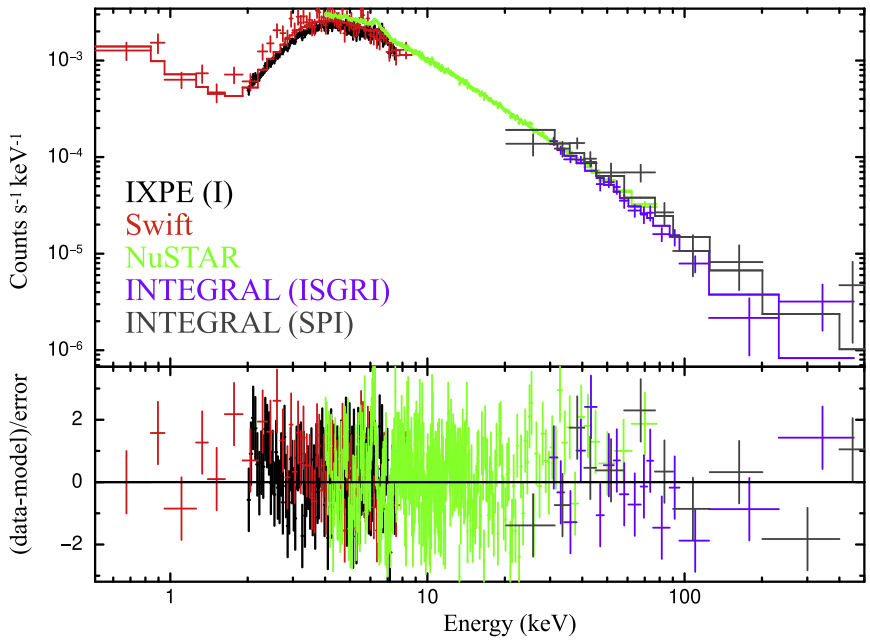

Figure 3. Model fit of the joint Swift (red), IXPE (black), NuSTAR (green), and INTEGRAL (purple and brown) X-ray spectrum of Cen A's core. This model corresponds to the simpler cutoff power-law model described in the text. No polarization information from IXPE is used in this model fit.

using other X-ray telescopes (e.g., Grandi et al. 2003; Evans et al. 2004; Markowitz et al. 2007; Fukazawa et al. 2011).

We added the second power-law component to fit the apparent residual counts observed at low energies (∼0.3–2.0 keV) when only fitting the data with a single power-law component. The best-fit photon index for this second component is $\Gamma = 1.21^{+0.06}_{-0.18}$, and its normalization is approximately 2 orders of magnitude lower than the primary component. Compared to a simpler model with only the primary power-law component, including a second power-law component reduces the total χ^2 value of the fit by a highly significant amount ($\Delta\chi^2 = -84$ with two fewer degrees of freedom). Converting this change in χ^2 into a change in Bayesian Information Criterion (BIC) for a model fit with 1150 data points and two additional parameters ($\Delta\mathrm{BIC} = 2\ln 1150 + \Delta\chi^2$) gives $\Delta\mathrm{BIC} = -69.9$, strongly favoring the presence of this second power law. The corresponding calculation for the Akaike Information Criterion (AIC) is $\Delta\mathrm{AIC} = 4 + \Delta\chi^2 = -80$, again validating the presence of this second power-law component. This component appears to be physically separated from the primary power law, as the data strongly disfavor a model where this second power-law component is subject to the same intrinsic absorption as the primary. We also attempted to fit these data to a similar model that replaces the second power law with a thermal `apec` model. An `apec` component is well motivated by the observed thermal emission in the vicinity of Cen A that would reside within the Swift point-spread function in the projection observed by Chandra (e.g., Kraft et al. 2003). The temperature and metallicity of this thermal component, however, cannot be well constrained by the spectral data. Fixing the temperature to $kT = 2.25$ keV and the metallicity to $0.4Z_\odot$ with a free normalization parameter enables a fit with χ^2 value statistically indistinguishable from our double power-law model.

As a further test of our spectral analysis, a BORUS component (e.g., Baloković et al. 2018, 2019) was included to self-consistently model the neutral Compton reflection and Fe line. In XSPEC the model reads as: `constant × tbabs × (atable(borus02_v170323l.fits) + atable(borus02_v170323k.fits) + ztbabs × cutoffpl) + pow`). The reflector is assumed to have a toroidal geometry and the opening angle is fixed to $\Delta\Omega/(4\pi) = 0.5$. The majority of the best-fit spectral parameters are broadly consistent with past measurements of Cen A obtained with NuSTAR (e.g., Fürst et al. 2016). In particular, we find that the Compton reflection can be well explained in terms of scattering off Compton-thin material, with a column density $\log(N_\mathrm{H}/\mathrm{cm}^{-2}) = 23.08^{+0.25}_{-0.15}$. Similar to our simpler model, the BORUS modeling finds no evidence for a high-energy cutoff. At 90% confidence the lower limit to the cutoff energy is $E_\mathrm{cut} > 590$ keV, and $E_\mathrm{cut} > 380$ keV at 99% confidence.

For both of the spectral model fits described above, the only parameter that strongly disagrees with the results of Fürst et al. (2016) is the normalization of the primary continuum, which is consistently a factor of ∼3–4 times lower than that calculated in Fürst et al. (2016). Such flux variations in this energy band are consistent with the factor of ∼3–4 variation of the 20–100 keV flux observed with the RXTE over a 12.5 yr period (Rothschild et al. 2011). As discussed in Fürst et al. (2016), the 2013 observation took place during a time when its flux was ∼40% higher than the average flux of Cen A measured between 2003 and 2009 with INTEGRAL (Beckmann et al. 2011).

3.3. Spectropolarimetric Fitting

We utilized the combined data from IXPE, NuSTAR, and Swift to perform a joint spectropolarimetric fit to the Cen A core emission, using a simpler version of our cutoff power-law model. The only modification is that the redshifted cutoff power-law model component is replaced with a simple power law, as there is no ability to constrain the cutoff energy without the INTEGRAL data. The polarization degree and angle are assumed to be constant with energy. In XSPEC this model is

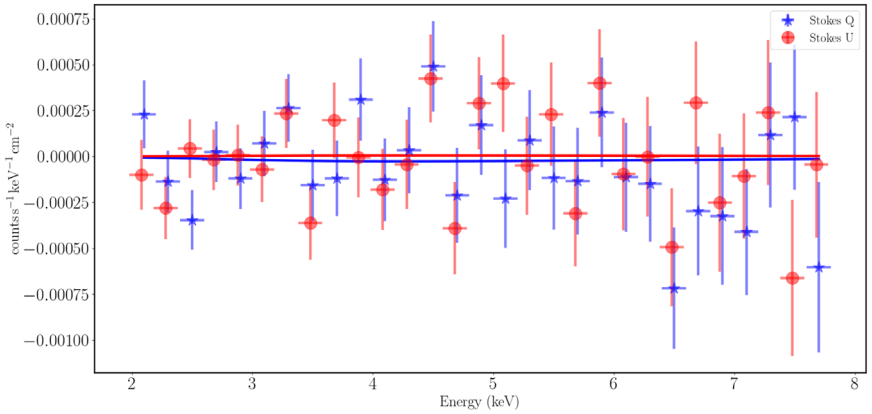

Figure 4. Spectropolarimetric model fit of the observed Stokes Q (in blue) and U (in red) spectra for Cen A. For presentation purposes, only the Q and U spectra have been slightly offset in energies. This model assumes a constant polarization degree and angle for the primary power-law continuum and an unpolarized Fe Kα line and secondary power law. This polarization model is determined simultaneously with the emission components (see main text for details). No statistically significant polarization is measured with this fit.

written as `const × tbabs × (ztbabs × (polconst × pow + polconst × zgauss) +polconst × pow )`. As stated above, no weighting was applied to the events when constructing the IXPE I, Q, and U spectra. The polarization degrees of the Gaussian component and second power law were fixed to zero, meaning that our upper limits are strictly for the primary power-law component.

We present three versions of the spectral fit: one allowing the polarization angle ψ to be fit as a free parameter, one where the polarization angle is fixed to $\psi = 55°$ (parallel to the radio jets), and one where $\psi = -35°$ (perpendicular to the radio jets in the relevant `XSPEC` coordinate system). When the polarization angle is a free parameter, the 99% confidence upper limit on the polarization degree is $\Pi < 8.0\%$. Fixing the polarization angles to $\psi = 55°$ or $\psi = -35°$ results in upper limits of $\Pi < 7.4\%$ and $\Pi < 6.2\%$, respectively. All other fit parameters are statistically consistent with those from the simpler spectral modeling performed above, and the χ^2 value of the fit (1259 for 1243 degrees of freedom) is in line with expectations for a "good" fit to the data. The IXPE Q and U spectra and the corresponding best-fit spectropolarmetric model are shown in Figure 4.

3.4. Summary of Results

We present the results of all six of the 99% confidence upper limits on the X-ray polarization of Cen A in Table 2. While all of these upper limits only differ from one another by a few percent, we choose to present the weighted value of MDP_{99} as the "primary" upper limit for Cen A's polarization. This choice arises from two facts of the weighted analysis. The first reason is that the value of MDP_{99} calculated with or without weights is independent of any assumptions or models for the SED. The second reason is that the weights have been designed and tested to increase the relative weight of events with reliable track reconstruction (Di Marco et al. 2022), therefore improving the sensitivity of the observation to polarization. This ∼10% reduction in MDP_{99} by using weights is in good agreement with expectations from prelaunch simulations (Baldini et al. 2022).

Table 2
Summary of all Calculations of the MDP_{99}

Method	Background	Weighting	ψ	99% Limit
PCUBE	None	None	Free	7.2%
PCUBE	None	N_{eff}	Free	6.5%
Likelihood	In Calculation	None	Free	7.1%
Spectropolarimetric	Subtracted	None	Free	8.0%
Spectropolarimetric	Subtracted	None	55°	7.4%
Spectropolarimetric	Subtracted	None	−35°	6.2%

Note. The PCUBE and Likelihood calculations are independent of any spectral model, while the spectropolarimetric calculations are dependent on the best-fit Cen A spectral model. For the model-independent calculations, the 99% limit is calculated as MDP_{99}, whereas for the model-dependent calculations, we use the model fits to determine 99% confidence upper limits on the polarization degree parameter.

4. Discussion

The apparent lack of a Compton hump suggests that the reflection component of the X-ray spectrum in Cen A arises primarily from reflection off an optically thin medium. On the other hand, the absence of any apparent cutoff in the power-law continuum agrees with past observations (e.g., Beckmann et al. 2011; Fürst et al. 2016). This differs from the typical X-ray spectrum of Type 1 AGN (e.g., Zdziarski et al. 1997, 2000; Fabian et al. 2015; Tortosa et al. 2018; Lanzuisi et al. 2019), where a cutoff is generally interpreted as the signature of Compton scattering of seed photons in a thermal corona. Assuming that spectrum is produced by thermal Comptonization, we can estimate the lower limit to the electron temperature from the lower limit on the cutoff energy as measured by INTEGRAL, as $kT \approx E_c/2 > 200$ keV (e.g., Stern et al. 1995; Petrucci et al. 2001; Middei et al. 2019). At such a high temperature, the Comptonization spectrum would deviate significantly from a single power law (Coppi 1999). This would suggest that thermal Comptonization is not the dominant process in producing the hard X-rays in Cen A and that nonthermal emission from the jet likely plays an important role. The spectrum extending beyond 511 keV, the rest-mass energy of the electron, would be prone to photon–photon electron–positron pair production, which would affect the shape of the spectrum. The absence of any significant features in the spectrum indicates that the source is not compact enough for this effect to play any role (Svensson 1994), adding further arguments in favor of the jet origin of the spectrum.

The variability of the different spectral components of Cen A between current and past observations (in particular those of Fürst et al. 2016) can provide additional information about the structure of the X-ray emission and central black hole. The lack of variability in the Fe Kα line (see also, e.g., Rothschild et al. 2011), despite the much higher variability in the continuum (e.g., Evans et al. 2004), is indicative of a scenario where the reflecting medium is not only optically thin but also quite distant from the region where the nonthermal X-rays are produced.

The upper limit to the degree of polarization measured by IXPE provides important information about the particle population responsible for generating the X-rays. Given the low polarization degrees measured for Cen A in the radio and IR bands, however, it is not surprising that significant polarization was not measured in the IXPE bandpass. Even using the optimistic assumption that the 11% polarization degree at 2 μm (Capetti et al. 2000) originates entirely from synchrotron radiation (hence dismissing any polar scattering contribution), our measured limits for the X-ray polarization degree remain consistent with expectations from synchrotron self-Compton emission, where the polarization degree of the Compton scattered X-rays is predicted to be $\sim$2–5 times smaller than that of the synchrotron radiation acting as seed photons for Compton scattering (Bonometto & Saggion 1973; Poutanen 1994; Celotti & Matt 1994; Peirson & Romani 2019). We note that Compton scattering of unpolarized seed photons, such as the Cosmic Microwave Background or starlight from the host galaxy of Cen A (Tanada et al. 2019) by isotropically distributed relativistic electrons in the jet would produce virtually unpolarized X-rays (Bonometto et al. 1970; Nagirner & Poutanen 1993; Poutanen 1994) because of relativistic aberration and resulting random rotation of polarization plane. Thus with a significantly longer exposure with IXPE, where MDP_{99} could reach levels of $\sim$1%, the detection of polarization would be a strong argument in favor of synchrotron radiation as a source of seed photons for Compton scattering. The increase in exposure time would be significant, however, as $\mathrm{MDP}_{99} \sim 4.29/\sqrt{N}$ for the total number of observed source events N. Assuming the same count rate for the IXPE observations presented here suggests a total of $\sim$5 Ms will be required to reach $\mathrm{MDP}_{99} \sim 1\%$. Even if future observations of Cen A were taken when the flux is a factor of $\sim$3 higher, we would still need $\sim$1.6–2 Ms to reach such an MDP_{99}. The observed limits on X-ray polarization are in tension with a physical scenario where the X-ray emission arises from hadronic jets. Processes involving hadrons in jets have been suggested as a possible source of the higher than expected emission of Cen A at TeV energies (Abdo et al. 2010; Joshi & Gupta 2013), and such models applied to blazars predict X-ray polarization degrees as high as $\sim$50%–80%, much higher than our limits allow (Zhang & Böttcher 2013).

All of the data presented in this work and in previous studies are consistent with a scenario where the majority of the X-rays observed in the core of Cen A originate from Compton scattering of lower-energy photons by nonthermal electrons, probably accelerated in regions within a few parsecs of the black hole. Since the polarization measurements for Cen A, spanning from radio to X-ray wavelengths, now sample both the synchrotron and Compton scattering components of the SED, it remains plausible that the nonthermal electrons are accelerated in a region in the core with disordered magnetic fields. The observed polarization of Cen A in the 2–100 microns wave band (Capetti et al. 2000; Lopez-Rodriguez 2021) likely arises from dichroic emission and absorption by aligned dust grains instead of direct emission from a nonthermal synchrotron component. Future studies of other AGN with IXPE will offer a clearer picture as to whether the low X-ray polarization degree observed in Cen A is typical of radio galaxies, or if it is an outlier among the radio galaxy population.

The Imaging X-ray Polarimetry Explorer IXPE is a joint US and Italian mission. The US contribution is supported by the National Aeronautics and Space Administration (NASA) and led and managed by its Marshall Space Flight Center (MSFC), with industry partner Ball Aerospace (contract NNM15AA18C). The Italian contribution is supported by the Italian Space Agency (Agenzia Spaziale Italiana, ASI) through contract ASI-OHBI-2017-12-I.0, agreements ASI-INAF-2017-12-H0 and ASI-INFN-2017.13-H0, and its Space Science Data Center (SSDC), and by the Istituto Nazionale di Astrofisica (INAF) and the Istituto Nazionale di Fisica Nucleare (INFN) in Italy. This research used data products provided by the IXPE Team (MSFC, SSDC, INAF, and INFN) and distributed with additional software tools by the High-Energy Astrophysics Science Archive Research Center (HEASARC) at NASA Goddard Space Flight Center (GSFC). We acknowledge Dawoon E. Kim for providing the polar plot script. J.R. acknowledges financial support under the INTEGRAL ASI-INAF agreement 2019-35-HH.0 and ASI/INAF No. 2019-35.HH.0. The research leading to these results has received funding from the European Union's Horizon 2020 Programme under the AHEAD2020 project(grant agreement n. 871158). The INTEGRAL SPI project has been completed under the responsibility and leadership of CNES. Part of the French contribution is supported by the Scientific Research National Center (CNRS) and the French spatial agency (CNES). We are grateful to ASI, CEA, CNES, DLR, ESA, INTA, NASA, and OSTC for their support. The research at Boston University was supported in part by the National Science Foundation grant AST-2108622.

ORCID iDs

Steven R. Ehlert https://orcid.org/0000-0003-1111-4292
Riccardo Ferrazzoli https://orcid.org/0000-0003-1074-8605
Andrea Marinucci https://orcid.org/0000-0002-2055-4946
Herman L. Marshall https://orcid.org/0000-0002-6492-1293
Riccardo Middei https://orcid.org/0000-0001-9815-9092
Luigi Pacciani https://orcid.org/0000-0001-6897-5996
Matteo Perri https://orcid.org/0000-0003-3613-4409
Pierre-Olivier Petrucci https://orcid.org/0000-0001-6061-3480
Simonetta Puccetti https://orcid.org/0000-0002-2734-7835
Thibault Barnouin https://orcid.org/0000-0003-1340-5675
Stefano Bianchi https://orcid.org/0000-0002-4622-4240
Ioannis Liodakis https://orcid.org/0000-0001-9200-4006
Frédéric Marin https://orcid.org/0000-0003-4952-0835
Alan P. Marscher https://orcid.org/0000-0001-7396-3332
Giorgio Matt https://orcid.org/0000-0002-2152-0916
Juri Poutanen https://orcid.org/0000-0002-0983-0049
Kinwah Wu https://orcid.org/0000-0002-7568-8765
Iván Agudo https://orcid.org/0000-0002-3777-6182
Matteo Bachetti https://orcid.org/0000-0002-4576-9337
Luca Baldini https://orcid.org/0000-0002-9785-7726
Ronaldo Bellazzini https://orcid.org/0000-0002-2469-7063
Raffaella Bonino https://orcid.org/0000-0002-4264-1215

Elisabetta Cavazzuti https://orcid.org/0000-0001-7150-9638
Stefano Ciprini https://orcid.org/0000-0002-0712-2479
Enrico Costa https://orcid.org/0000-0003-4925-8523
Ettore Del Monte https://orcid.org/0000-0002-3013-6334
Alessandro Di Marco https://orcid.org/0000-0003-0331-3259
Victor Doroshenko https://orcid.org/0000-0001-8162-1105
Michal Dovčiak https://orcid.org/0000-0003-0079-1239
Teruaki Enoto https://orcid.org/0000-0003-1244-3100
Sergio Fabiani https://orcid.org/0000-0003-1533-0283
Javier A. Garcia https://orcid.org/0000-0003-3828-2448
Jeremy Heyl https://orcid.org/0000-0001-9739-367X
Wataru Iwakiri https://orcid.org/0000-0002-0207-9010
Svetlana G. Jorstad https://orcid.org/0000-0001-6158-1708
Vladimir Karas https://orcid.org/0000-0002-5760-0459
Henric Krawczynski https://orcid.org/0000-0002-1084-6507
Fabio La Monaca https://orcid.org/0000-0001-8916-4156
Luca Latronico https://orcid.org/0000-0002-0984-1856
Simone Maldera https://orcid.org/0000-0002-0698-4421
Alberto Manfreda https://orcid.org/0000-0002-0998-4953
Francesco Massaro https://orcid.org/0000-0002-1704-9850
Tsunefumi Mizuno https://orcid.org/0000-0001-7263-0296
Fabio Muleri https://orcid.org/0000-0003-3331-3794
Michela Negro https://orcid.org/0000-0002-6548-5622
C.-Y. Ng https://orcid.org/0000-0002-5847-2612
Nicola Omodei https://orcid.org/0000-0002-5448-7577
Alessandro Papitto https://orcid.org/0000-0001-6289-7413
George G. Pavlov https://orcid.org/0000-0002-7481-5259
Abel L. Peirson https://orcid.org/0000-0001-6292-1911
Melissa Pesce-Rollins https://orcid.org/0000-0003-1790-8018
Maura Pilia https://orcid.org/0000-0001-7397-8091
Andrea Possenti https://orcid.org/0000-0001-5902-3731
John Rankin https://orcid.org/0000-0002-9774-0560
Roger W. Romani https://orcid.org/0000-0001-6711-3286
Carmelo Sgrò https://orcid.org/0000-0001-5676-6214
Patrick Slane https://orcid.org/0000-0002-6986-6756
Paolo Soffitta https://orcid.org/0000-0002-7781-4104
Fabrizio Tavecchio https://orcid.org/0000-0003-0256-0995
Sergey Tsygankov https://orcid.org/0000-0002-9679-0793
Roberto Turolla https://orcid.org/0000-0003-3977-8760
Jacco Vink https://orcid.org/0000-0002-6384-3027
Martin C. Weisskopf https://orcid.org/0000-0002-5270-4240
Elisabeth Jourdain https://orcid.org/0000-0001-9932-3288
Jean-Pierre Roques https://orcid.org/0000-0002-6529-4121

References

Abdo, A. A., Ackermann, M., Ajello, M., et al. 2010, ApJ, 719, 1433
Arnaud, K. A. 1996, in ASP Conf. Ser. 101, Astronomical Data Analysis Software and Systems V, ed. G. H. Jacoby & J. Barnes (San Francisco, CA: ASP), 17
Baldini, L., Bucciantini, N., Di Lalla, N., et al. 2022, arXiv:2203.06384
Baloković, M., Brightman, M., Harrison, F. A., et al. 2018, ApJ, 854, 42
Baloković, M., García, J. A., & Cabral, S. E. 2019, RNAAS, 3, 173
Beckmann, V., Jean, P., Lubiński, P., Soldi, S., & Terrier, R. 2011, A&A, 531, A70
HI4PI Collaboration, Ben Bekhti, N., Flöer, L., et al. 2016, A&A, 594, A116
Bonometto, S., Cazzola, P., & Saggion, A. 1970, A&A, 7, 292
Bonometto, S., & Saggion, A. 1973, A&A, 23, 9
Burke, M. J., Jourdain, E., Roques, J.-P., & Evans, D. A. 2014, ApJ, 787, 50
Burns, J. O., Feigelson, E. D., & Schreier, E. J. 1983, ApJ, 273, 128
Capetti, A., Schreier, E. J., Axon, D., et al. 2000, ApJ, 544, 269
Celotti, A., & Matt, G. 1994, MNRAS, 268, 451
Clarke, D. A., Burns, J. O., & Feigelson, E. D. 1986, ApJL, 300, L41
Coppi, P. S. 1999, in ASP Conf. Ser. 161, High Energy Processes in Accreting Black Holes, ed. J. Poutanen & R. Svensson (San Francisco, CA: ASP), 375
Di Marco, A., Costa, E., Muleri, F., et al. 2022, AJ, 163, 170
Elsner, R. F., O'Dell, S. L., & Weisskopf, M. C. 2012, Proc. SPIE, 8443, 84434N
Evans, D. A., Kraft, R. P., Worrall, D. M., et al. 2004, ApJ, 612, 786
Fabian, A. C., Lohfink, A., Kara, E., et al. 2015, MNRAS, 451, 4375
Ferrazzoli, R., Muleri, F., Lefevre, C., et al. 2020, JATIS, 6, 048002
Fukazawa, Y., Hiragi, K., Yamazaki, S., et al. 2011, ApJ, 743, 124
Fürst, F., Müller, C., Madsen, K. K., et al. 2016, ApJ, 819, 150
Goddi, C., Martí-Vidal, I., Messias, H., et al. 2021, ApJL, 910, L14
Grandi, P., Fiocchi, M., Perola, C. G., et al. 2003, ApJ, 593, 160
Hardcastle, M. J., Worrall, D. M., Kraft, R. P., et al. 2003, ApJ, 593, 169
Janssen, M., Falcke, H., Kadler, M., et al. 2021, NatAs, 5, 1017
Jones, D. L., Tingay, S. J., Murphy, D. W., et al. 1996, ApJL, 466, L63
Joshi, J. C., & Gupta, N. 2013, PhRvD, 87, 023002
Kinzer, R. L., Johnson, W. N., Dermer, C. D., et al. 1995, ApJ, 449, 105
Kislat, F., Clark, B., Beilicke, M., & Krawczynski, H. 2015, APh, 68, 45
Kraft, R. P., Vázquez, S. E., Forman, W. R., et al. 2003, ApJ, 592, 129
Lanzuisi, G., Gilli, R., Cappi, M., et al. 2019, ApJL, 875, L20
Lopez-Rodriguez, E. 2021, Nature Astronomy, 5, 604
Markowitz, A., Takahashi, T., Watanabe, S., et al. 2007, ApJ, 665, 209
Marshall, H. L. 2021, ApJ, 907, 82
Middei, R., Bianchi, S., Marinucci, A., et al. 2019, A&A, 630, A131
Müller, C., Kadler, M., Ojha, R., et al. 2014, A&A, 569, A115
Nagirner, D. I., & Poutanen, J. 1993, A&A, 275, 325
Peirson, A. L., & Romani, R. W. 2019, ApJ, 885, 76
Petrucci, P. O., Haardt, F., Maraschi, L., et al. 2001, ApJ, 556, 716
Poutanen, J. 1994, ApJS, 92, 607
Rankin, J., Muleri, F., Tennant, A. F., et al. 2022, AJ, 163, 39
Rothschild, R. E., Markowitz, A., Rivers, E., et al. 2011, ApJ, 733, 23
Schreier, E. J., Feigelson, E., Delvaille, J., et al. 1979, ApJL, 234, L39
Soffitta, P., Baldini, L., Bellazzini, R., et al. 2021, AJ, 162, 208
Steinle, H., Bennett, K., Bloemen, H., et al. 1998, A&A, 330, 97
Stern, B. E., Poutanen, J., Svensson, R., Sikora, M., & Begelman, M. C. 1995, ApJL, 449, L13
Svensson, R. 1994, ApJS, 92, 585
Tanada, K., Kataoka, J., & Inoue, Y. 2019, ApJ, 878, 139
Tingay, S. J., Preston, R. A., & Jauncey, D. L. 2001, AJ, 122, 1697
Tortosa, A., Bianchi, S., Marinucci, A., Matt, G., & Petrucci, P. O. 2018, A&A, 614, A37
Weisskopf, M. C., Ramsey, B., O'Dell, S., et al. 2016, Proc. SPIE, 9905, 990517
Weisskopf, M. C., Soffitta, P., Baldini, L., et al. 2022, JATIS, 8, 026002
Zdziarski, A. A., Johnson, W. N., Poutanen, J., Magdziarz, P., & Gierlinski, M. 1997, in ESA Special Publication, Vol. 382, The Transparent Universe, ed. C. Winkler, T. J. L. Courvoisier, & P. Durouchoux (Paris: ESA), 373
Zdziarski, A. A., Poutanen, J., & Johnson, W. N. 2000, ApJ, 542, 703
Zhang, H., & Böttcher, M. 2013, ApJ, 774, 18